Progress In Electromagnetics Research C, Vol. 150, 17-26, 2024

PIER C

(Received 5 July 2024, Accepted 23 October 2024, Scheduled 5 November 2024)

Controllable Multimode Four-Passband Filter Based on Substrate-Integrated Waveguide

Mingming Gao[1,2], Congying Wang[1,2,*], Jingchang Nan[1,2], Xinyu Wang[1,2], and Ya He[1,2]

[1] *College of Electronics and Information Engineering, Liaoning Technicial University, Huludao, Liaoning Province, China*
[2] *Liaoning Key Laboratory of Radio Frequency and Big Data for Intelligent Applications, China*

ABSTRACT: A metalized through-hole perturbation structure is proposed to effectively control multiple modes of substrate-integrated waveguide (SIW) filters. The method manipulates six modes (TE_{101}, TE_{201}, TE_{102}, TE_{202}, TE_{301}, and TE_{401}), result in the formation of three passbands. Subsequently, two symmetrical parallel complementary split ring resonators (CSRRs) are introduced without altering the filter's size. These rings generate resonances primarily excited by TE_{201} and TE_{102}, allowing the filter to produce a fourth passband. Additionally, extra transmission zeros (TZs) are added, creating a perturbing effect on other modes. This further aids in controlling the resonances of these modes. The filter exhibits flexibility and controllability in terms of center frequency, bandwidth, and transmission zeros. The center frequencies of the four passbands are measured at 7.47 GHz, 9.84 GHz, 11.02 GHz, and 12.65 GHz, with return losses exceeding 18 dB. Additionally, there are six TZs, with the highest frequency point reaching -56.58 dB, indicating good in-band and out-of-band rejection. The measured and simulated results demonstrate satisfactory performance and applicability to multi-channel transmission in radar and satellite communication systems.

1. INTRODUCTION

Over the past century, communications technology has rapidly been developed and led to significant changes [1]. Modern communication, surveillance, and navigation systems are crucial due to the continuous advancement of radar and satellite communication technologies. Radar technology enables the detection and monitor of objects and substances from a distance, even in challenging visibility conditions. Conversely, satellite communication technologies enable global communication over long distances, regardless of whether it is in urban, rural, or remote areas. They provide fast, reliable telephone, Internet, and data transmission services for applications across various fields, including aviation, military operations, meteorology, and law enforcement. For instance, radar and satellite communication systems in aviation play a pivotal role in aircraft detection, tracking, and air traffic control [2]. Moreover, in meteorology, radar and satellite systems detect weather phenomena like rainfall, snowfall, and hurricanes, assisting scientists and meteorologists in conducting climate analyses and forecasts to provide precise weather forecasts and warnings for the protection of lives and property [3]. In radar and satellite communication systems, a fundamental aspect of signal processing is filter technology, with a particular emphasis on multi-passband filters. Multi-passband filters are essential for transmitting signals within a specific frequency range, and their applications encompass various crucial aspects of radar and communication systems [4, 5].

The predominant approach in designing multi-passband filters involves the utilization of stepped impedance resonators (SIRs) [6, 7]. Although the used SIR microstrip structure filter has low cost and high interband isolation, it is difficult to meet the requirements of most radar and satellite communication systems due to its low figure of merit. This is because the complexity of the SIR filter structure and the resonance mode can lead to limitations in energy loss and isolation, especially in high-frequency applications. The design of SIW filter allows for precise control of the distribution and coupling of the electromagnetic field. By optimizing the design, the coupling between adjacent modes can be minimized, and mutual interference can be reduced, resulting in higher Q values. The Q factor of a SIW filter can be many times higher than that of a SIR filter, depending on the specific design and manufacturing process [8]. To enhance the selectivity and out-of-band rejection of multipass band-pass filters, scholars have conducted extensive research. As a result, several design methods for multipassband substrate-integrated waveguide filters have been proposed.

A comprehensive design method for substrate-integrated waveguide (SIW) multiband band-pass filters is proposed in [9]. The method is based on various combinations of split dual- or triple-band symmetric frequency responses of two virtual wide bands, composed of TE_{101} and TE_{201} modes in Substrate Integrated Resonant Cavities (SIRC). This theoretical framework enables the realization of SIW triple/quad/quintuple/hexa-band bandpass filters with enhanced frequency and bandwidth allocation. The implementation method integrates coupled matrix splitting techniques

* Corresponding author: Congying Wang (903267979@qq.com).

and the use of dual-mode resonators to provide an effective solution for multiband bandpass filters in substrate-integrated waveguides. While this approach yields a perfectly symmetric frequency response, the subpassbands are often closely adjacent, posing challenges for independent assignment or control. A novel dual-band filter was proposed in [10, 11] by combining substrate-integrated waveguide (SIW) and microstrip techniques to achieve a quasi-elliptical response in both passbands. However, the design may lead to some flexibility limitations despite combining the two techniques. It will be challenging to tune or optimize the performance for a specific frequency band, and the adaptability for different application scenarios may be affected. Refs. [12, 13] divide a wide passband into multiple sub-passbands by inserting transmission zeros (TZs), but only a limited number of frequency ratios can be achieved. In [14–17], three-mode band-pass filters (BPFs) were proposed based on three-mode BPFs with symmetric perturbation cavities. However, due to the symmetric structure of the three-mode cavities, the second-order and third-order modes are merged, making independent tuning impossible. Additionally, more perturbations must be added to separate them, resulting in a more complex structure. To address issues related to the excessive size and design flexibility of the filter, [18–21] proposed a multilayer filter structure, incorporating two vertically stacked SIW resonators. The coupling between these resonant cavities is established through grooved lines on their respective contact surfaces, working in conjunction with the resonant modes of these lines. Passbands can emerge through the coupling of multiple modes. The design features a simple structure, compact size, and ease of integration. However, the passbands lack independence, and the copper layer on the contact surfaces of the upper and lower resonant cavities may impact the coupling effect, rendering the processing both costly and challenging [22, 23].

In this paper, we propose a flexible and controllable substrate-integrated waveguide structure to address the shortcomings of the existing literature. Additionally, a four-passband filter with effective in-band and out-of-band rejection is designed based on this structure. Introducing a metallized through-hole perturbation structure at the center of the substrate-integrated waveguide cavity enables independent tunability of the resonance frequencies for six modes: TE_{101}, TE_{201}, TE_{102}, TE_{202}, TE_{301}, and TE_{401}. This demonstrates the flexibility of the multi-passband design. At the same time, while maintaining the overall size of the cavity, a pair of symmetrical circular Complementary Split-Ring Resonator (CSRRs) is integrated into the upper metal plate using the proposed disturbance multimode substrate integrated waveguide cavity. The ring structure serves both as a resonator and as a micro-perturbation element, and an additional transmission zero is introduced to achieve the desired bandwidth and isolation. The final designed four-passband filter structure allows for flexible adjustment of the resonant frequency, bandwidth, stopband width between bands, and the position of the transmission zero, while providing excellent in-band and out-of-band suppression. This makes the filter well suited for multi-channel transmission in radar and satellite communication systems.

2. PERTURBATIVE MULTIMODE STRUCTURES FOR SUBSTRATE-INTEGRATED WAVEGUIDES

In general, the resonant mode of a single substrate-integrated waveguide resonator can be initially tuned using its two sides to estimate the approximate frequencies of multiple modes. The resonant frequency Equation (1) for the TE_{m0n} mode is as follows:

$$F_{TE_{m0n}} = \frac{c}{2\sqrt{\mu_r \epsilon_r}} \sqrt{\frac{m^2}{W_{\mathit{eff}}} + \frac{n^2}{L_{\mathit{eff}}}} \tag{1}$$

where c is the speed of light in vacuum; μ_r and ϵ_r are the relative permeability and relative permittivity, respectively; m and n are the mode indices along the cavity in both directions, respectively, with $m, n = 0, 1, 2 \ldots$; and W_{eff} and L_{eff} are the width and length equivalent to the metal rectangular waveguide, respectively.

This paper proposes a multimode substrate-integrated waveguide cavity with a perturbed structure to achieve independently controllable multimode resonant modes. Metalized apertures are loaded at the center of the structure to constitute a multimode resonant cavity. Figure 1(a) illustrates a circular metalized perforation with a radius R_1 at the center of the rectangular substrate-integrated waveguide. Additional metallized perforations are also positioned at the horizontal sides of the structure to further regulate the variation of the multimode resonance. The paper presents the electric field distributions of six modes, as illustrated in Figure 1(b). The metal perforated structure is positioned at TE_{101}, TE_{102}, and TE_{301}, where the electric field strengths are larger and are significantly affected by the perturbation effect of the metal perforations. However, these modes experience only slight perturbation since the structure is almost at zero electric fields for TE_{201}, TE_{202}, and TE_{401}.

The analysis of the structure's parameters aimed to illustrate the effects of metal perforations on modes and frequencies. Figure 2(a) portrays the relationship between the magnitude of R_1 and the change in frequency. The resonant frequencies of TE_{101} and TE_{201} gradually increase with an increase in R_1, approaching each other, thereby forming a passband. Likewise, the resonant frequency of TE_{102} gradually increases with an increase in R_1, approaching TE_{202}, forming a passband. Changes in R_1 minimally affect the frequency of TE_{202} due to the distribution of the electric field position. Meanwhile, the frequencies of TE_{301} and TE_{401} gradually increase with an increase in R_1, but their resonant frequencies are not closely aligned with each other. Figures 2(b) and (c) demonstrate the impact of the external metal through-hole on the modes' characteristics. As P_1 increases from 0 to 4 mm while P_2 remains fixed and unchanged, the resonance frequencies of TE_{101}, TE_{102}, and TE_{301} shift towards the resonance frequencies of TE_{201}, TE_{202}, and TE_{401} modes, respectively. Similarly, when P_2 is increased to 3 mm while P_1 remains unchanged, the resonance frequencies of TE_{101}, TE_{102}, and TE_{301} gradually move towards the resonance frequencies of TE_{201}, TE_{202}, and TE_{401} modes, respectively. As both P_1 and P_2 continue to increase, the resonant frequencies of TE_{101}, TE_{102}, and TE_{401} modes decrease.

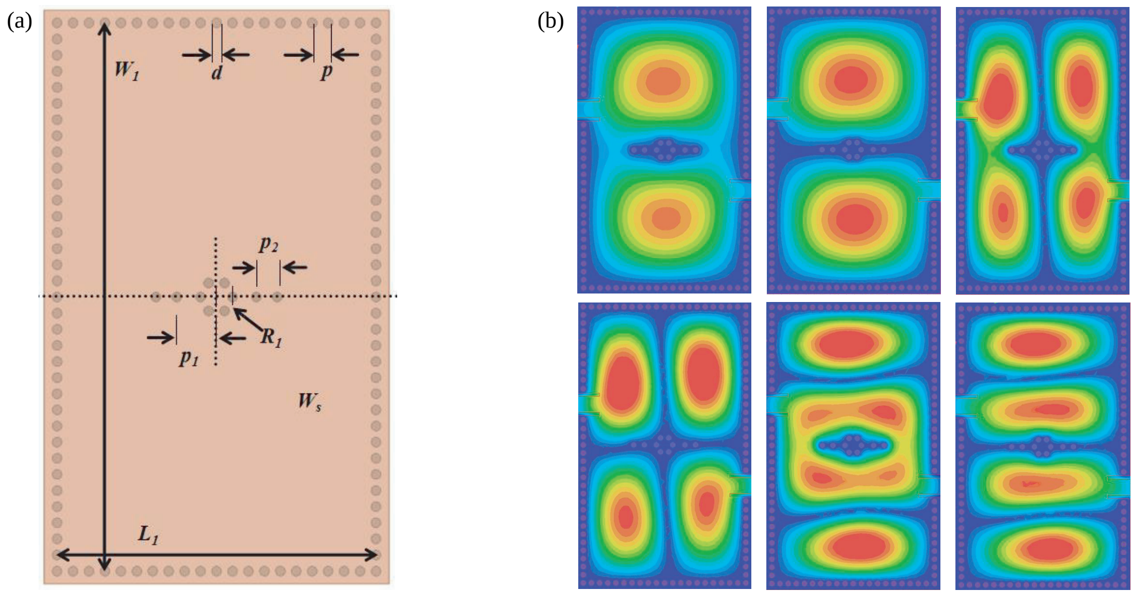

FIGURE 1. Substrate integrated waveguide metal perturbation structure. (a) Geometry. (b) The electric field pattern from left to right from top to bottom is TE_{101}, TE_{201}, TE_{102}, TE_{202}, TE_{301} and TE_{401}.

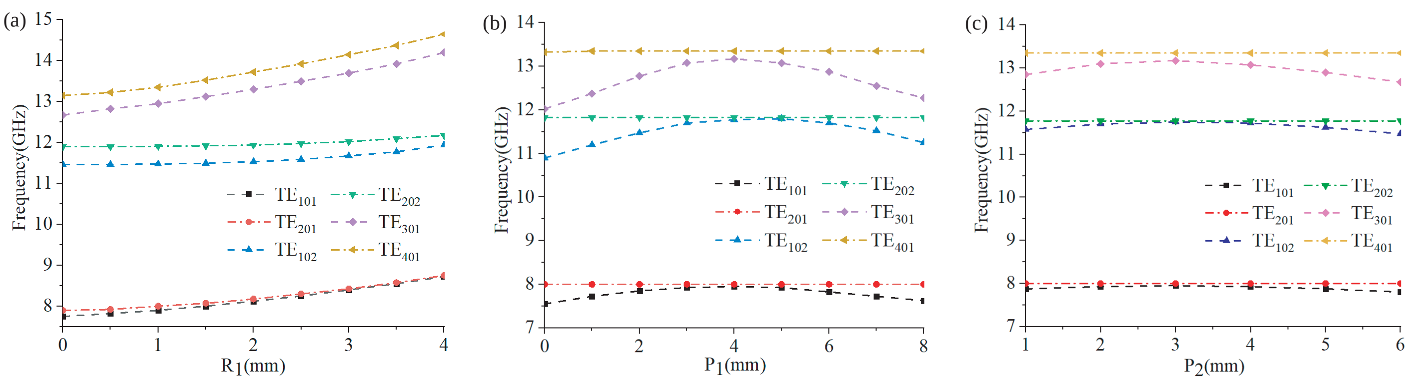

FIGURE 2. Effects of metal vias on the resonant mode. (a) R_1 and on the resonant mode. (b) P_1 and on the resonant mode. (c) P_2 and on the resonant mode.

Figure 3(a) displays the S-curve of R_1, illustrating that the structure can be manipulated to generate three passbands. With the increase of R_1, the frequency of the first passband gradually rises, whereas the frequency of the second passband initially increases before reaching stability. The relative bandwidths of the initial two passbands gradually diminish. The TE_{301} and TE_{401} modes gradually combine to create the third passband, accompanied by increasing relative bandwidths and transmission zeros shifting to the right. Figure 3(b) illustrates that as P_1 and P_2 increase, the center frequencies of the three generated passbands initially ascend and subsequently descend concurrently. The relative bandwidth initially diminishes and then enlarges concurrently, while the transmission zeros shift to the right.

The quality factor of the filter can be influenced by the metal vias of the substrate-integrated waveguide. Consequently, correlation curves were derived between the parameters of the perturbed metal vias and quality factor, as depicted in Figure 4.

3. FOUR-PASS BAND FILTER DESIGN BASED ON RESONANT RING STRUCTURE

Split ring resonator (SRR) technology was initially applied to structural units of left-handed materials. These units comprise two square metal ring openings that are nested relative to each other. The complementary SRR (CSRR) is achieved by etching the SRR structure shape into the metal plane, producing results similar to those of left-handed materials. This is when both the dielectric constant and the magnetic permeability are negative simultaneously [24, 25]. Figure 5(a) illustrates the circular CSRR, with the metal part in orange and CSRR structure in white. The metal layer on the dielectric substrate is etched to form the CSRR structure. The outer ring has a radius of R_2; the etched line's width is W_d; the ring spacing is W_g; and the ring opening is W_c.

The circular complementary resonant ring possesses a unique resonance property, and its resonant frequency can be tuned by modifying its geometrical parameters within a specified mi-

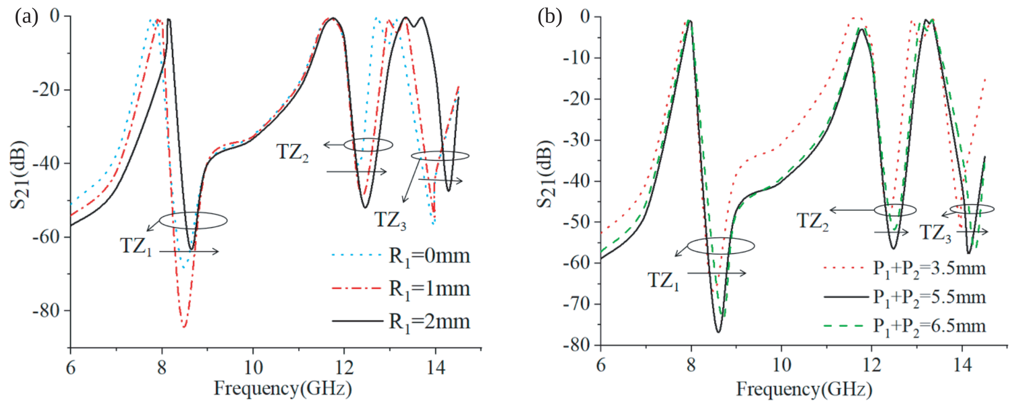

FIGURE 3. Effects of metal vias on S parameters. (a) Effects of R_1 on S parameters. (b) Effects of P_1 and P_2 on S parameters.

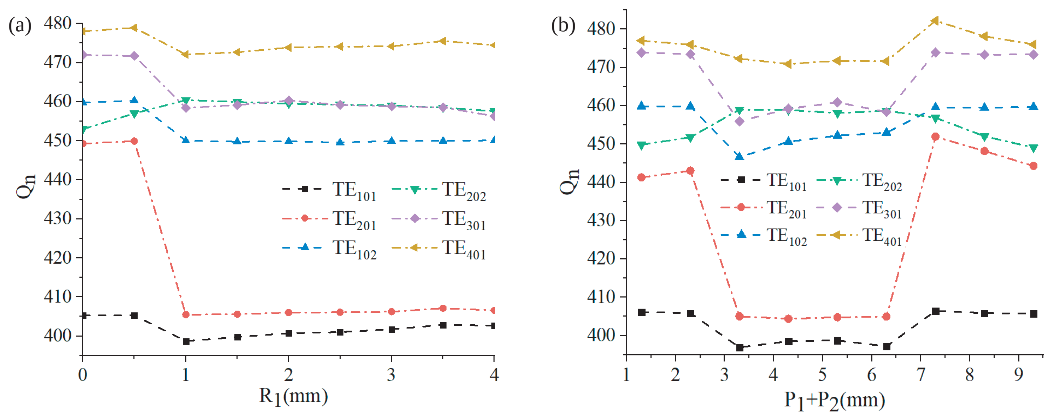

FIGURE 4. Relationship between metal vias and quality factor. (a) Relationship between R_1 and quality factor Q. (b) Relationship between P_1 and P_2 and quality factor Q.

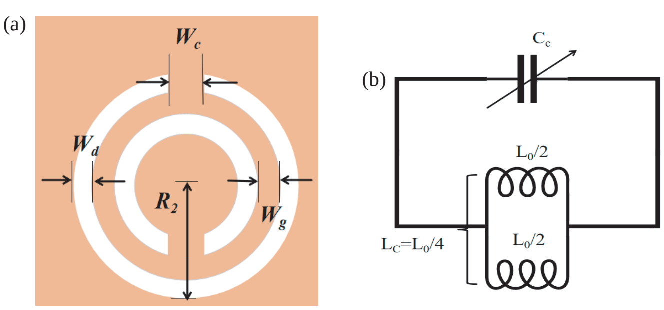

FIGURE 5. The structure of the complementary opening resonant ring. (a) The basic structure. (b) The equivalent topology.

crowave or radio frequency (RF) range. The metal-to-metal contact within the ring results in a capacitance denoted as C_c, and the metal situated between the inner and outer rings gives rise to an induced inductance denoted as L_c. The equivalent topology is depicted in Figure 5(b), wherein L_0 can be expressed as:

$$L_0 = 2\pi r L_{pul} \tag{2}$$

where L_{pul} is the inductance per unit length between the rings, and r is the inner ring radius, expressed as:

$$r = R_2 - W_d - W_g \tag{3}$$

and the expression for C_c is:

$$C_c = \frac{4\epsilon_0 L_s}{\mu_0} \tag{4}$$

L_s denotes the total equivalent inductance of the complementary structure SRR corresponding to the CSRR, which is the sum of the intrinsic inductance L_p of the SRR double ring and the mutual inductance L_m between the double rings, respectively:

$$L_p = \mu_0 \left[\left(1 + \frac{3\xi^2}{4} \right) \log \frac{4}{\xi} - 2 \right] \tag{5}$$

Therefore, the resonant frequency of CSRR is:

$$F_{\text{CSRR}} = \frac{1}{2\pi\sqrt{L_0 C_0}} \tag{6}$$

The paper introduces a band-pass filter design employing two-ring CSRRs with opposite openings on the upper metal plate. The geometry and topology of the proposed quad-band filter are illustrated in Figure 6. Node 1 and node 2 represent the TE_{101} and TE_{201} modes, forming the first passband collectively. Figure 6(c) illustrates the resonant electric field mode

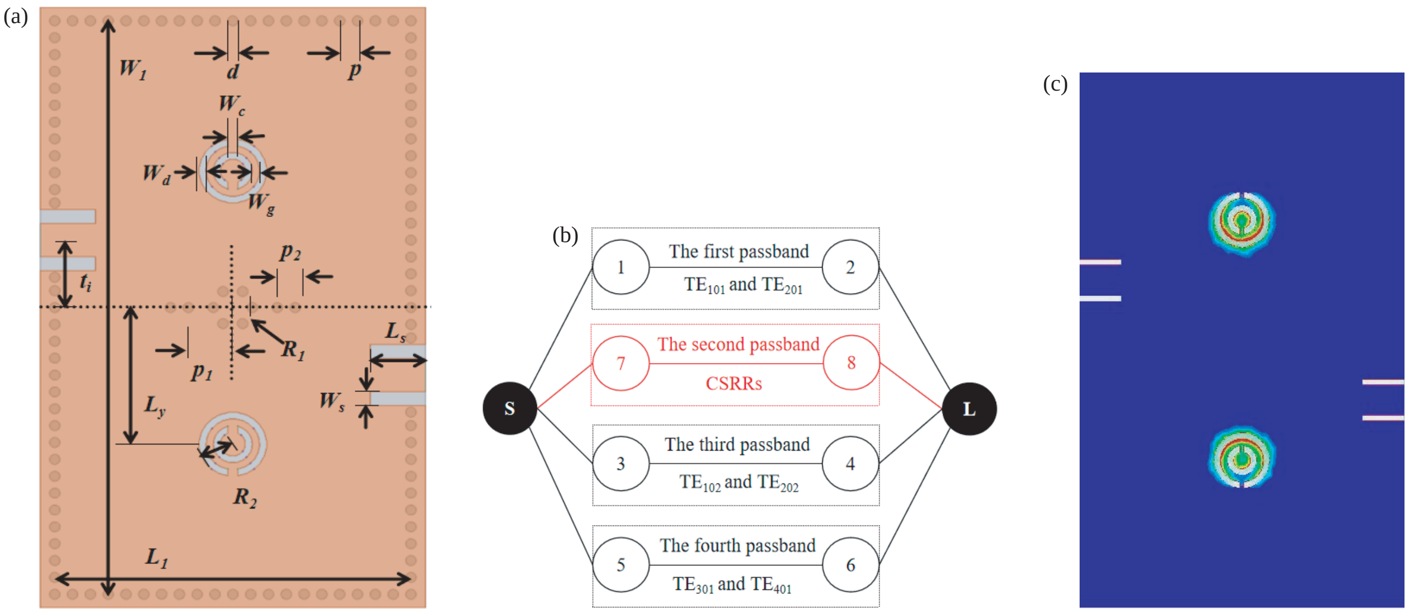

FIGURE 6. Four-passband filter structure. (a) Geometry. (b) Coupling topology. (c) The electric field distribution of the second passband.

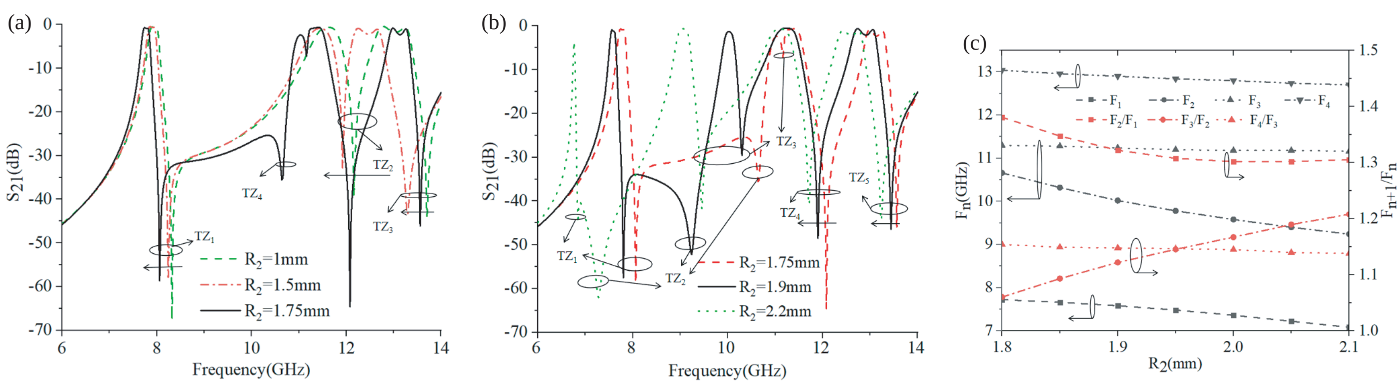

FIGURE 7. Effect of the CSRRs etching ring radius R_2 on the filter. (a) S parameters when R_2 is less than 1.75 mm. (b) S parameters when R_2 is more than 1.75 mm. (c) R_2 versus frequency variation.

for the second passband, which is produced by the resonant frequency of the CSRRs functioning between the TE_{201} and TE_{102} modes. Nodes 7 and 8 denote the resonant modes of the two CSRRs. Nodes 3 and 4 represent the TE_{102} and TE_{202} modes, respectively. The TE_{102} mode shifts towards the TE_{202} mode to form a third passband. Nodes 5 and 6 represent the TE_{301} and TE_{401} modes, respectively; these modes shift to form the fourth passband. The CSRRs are positioned at the zero electric field distribution of the TE_{102} and TE_{202} modes, causing slight changes in the resonant frequencies of these modes. This structure achieves four passbands and improves out-of-band rejection by incorporating additional transmission zeros. It also enhances the performance of microwave circuits without increasing their footprint, achieving device miniaturization.

According to the provided equation and theory, it is evident that the resonant frequency generated by the CSRRs is controllable based on its dimensions. Based on calculations and the utilization of three-dimensional electromagnetic simulation software, Ansys Electronics Desktop, the results are as follows: if the radius (R_2) of the CSRRs is less than 1.75 mm, the resonant point that it generates merges with the third passband. Figure 7(a) and Table 1 illustrate that with an increase in R_2, the center frequencies of the three bands shift towards lower frequencies; the relative bandwidths decrease; and the three transmission zeros relocate to lower frequencies. Consequently, the primary effect of the CSRRs is to induce a minor perturbation in the passbands. When the radius (R_2) of the CSRRs exceeds 1.75 mm, the resonance point produced by the CSRRs continues shifting towards lower frequencies. Consequently, it diverges from the third passband, resulting in the presence of four passbands in the filter, as depicted in Figure 7(b) and Table 1. As R_2 increases, the center frequency of these four bands shifts to lower frequencies, accompanied by a corresponding movement of the resulting transmission zeros. At this stage, the primary function of the CSRRs is to induce resonance and induce a minor perturbation in the remaining passbands. It is noteworthy that if the etch radius (R_2) becomes excessively large, the transmission zeros located to the right of the first passband

TABLE 1. Effect of CSRRs etch ring radius R_2 on filter parameters.

Cases	R_2 (mm)	Passband	Frequency (GHz)	FBW (%)
Case 1	1	The first passband	7.94	2.64
		The second passband	11.62	4.39
		The third passband	13.04	5.52
Case 2	1.5	The first passband	7.90	2.28
		The second passband	11.44	4.02
		The third passband	12.44	4.82
Case 3	1.75	The first passband	7.76	1.93
		The second passband	11.04	1.18
		The third passband	11.36	3.00
		The fourth passband	13.14	3.04
Case 4	1.9	The first passband	7.58	1.45
		The second passband	10.02	1.80
		The third passband	11.24	4.27
		The fourth passband	12.90	3.80
Case 5	2.2	The first passband	6.76	IL (dB) < -3 dB
		The second passband	9.04	2.65
		The third passband	11.10	3.87
		The fourth passband	12.58	4.05

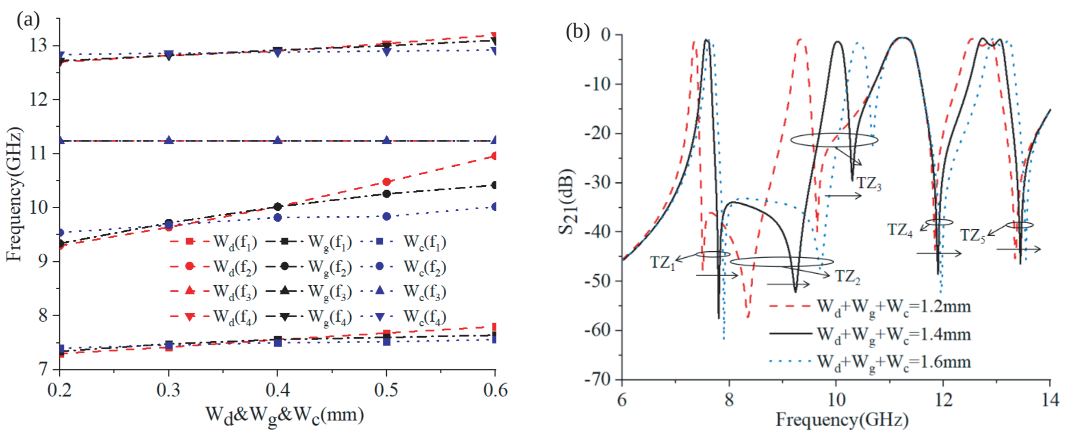

FIGURE 8. The influence of the internal parameters of the etching ring on the filter. (a) The relationship between the internal parameters of the etching ring and the frequency of each mode. (b) The relationship between the internal parameters of the etching ring and the corresponding S.

shift towards lower frequencies, leading to an excessive suppression beyond the passband and significantly impacting the performance of the first passband.

This paper focuses on four-passband filters, driven by the societal demand for multi-passband transmission systems. Figure 7(c) illustrates the frequency change characteristics of parameter R_2 and the relationship between its ratios. With an increase in R_2, the center frequency of the second passband shifts to lower frequencies, and the remaining three passbands are perturbed slightly to lower frequencies. The ratio of frequencies between the second and first passbands initially decreases before stabilizing. The ratio between the frequencies of the third and second passbands increases gradually. The ratio between the frequencies of the fourth and third passbands remains almost unchanged. This is due to the electric fields of the TE_{102} and TE_{202} modes being zero along the perpendicular center line, resulting in the center frequency of the third passband being almost unaffected by the CSRR.

Figure 8 illustrates that increasing the line width (W_g) and ring spacing (W_d) of the etched ring decreases the value of the shunt resonant capacitance, thereby shifting the resonant frequency point and transmission zero towards higher frequencies, thus enhancing out-of-band rejection. Adjusting W_c has a minor effect on the filter compared to adjusting W_g and W_d. Increasing W_c reduces the shunt resonant inductance and slightly shifts the zero point towards higher frequencies. The internal parameters of the etch ring primarily affect the second passband and perturb the first and fourth passbands. Since the etched ring is positioned at the point of the weakest electric field pattern in the third passband, internal parameters have minimal impact.

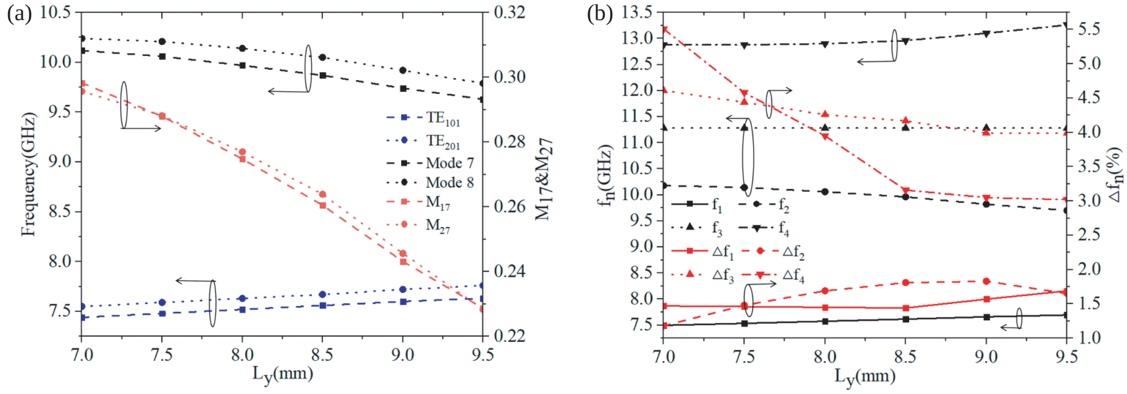

FIGURE 9. Effect of offset L_y on the filter. (a) Effect of L_y on resonance modes and coupling coefficients. (b) Frequency and relative bandwidth of L_y vs.

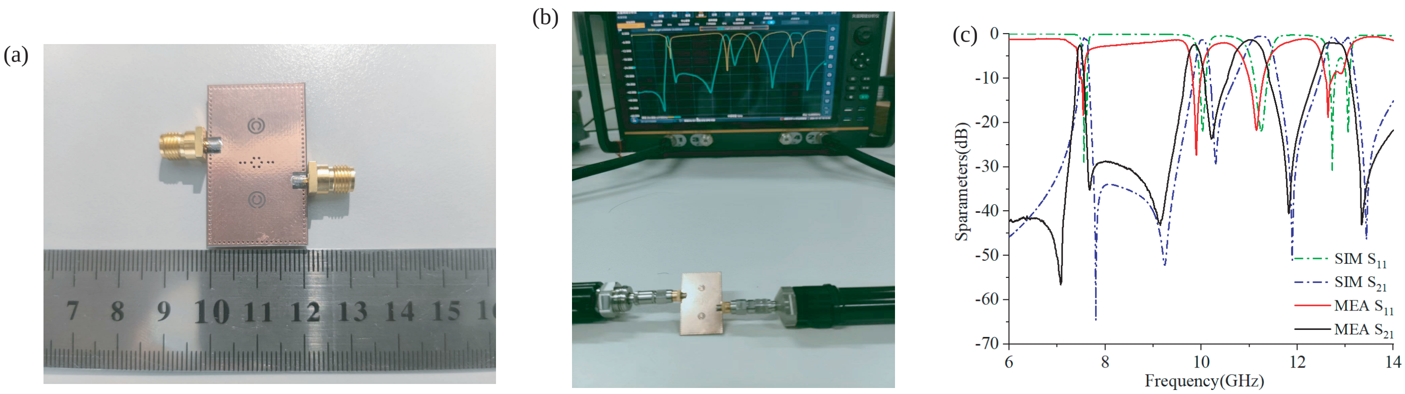

FIGURE 10. Physical measurement results. (a) Physical drawing. (b) Vector-net analyzer test drawing. (c) Filter simulation and measurement results.

To illustrate the effect of the offset L_y on the filter, Figure 9(a) displays the resonant frequencies of the CSRRs and their coupling coefficients with respect to L_y. As L_y increases, the resonant frequencies of TE_{101} and TE_{201} gradually rise, whereas those of the CSRRs gradually decline. Consequently, the first passband shifts to a higher frequency, while the second passband shifts to a lower one. The coupling coefficients M_{17} and M_{27} decrease with increasing L_y. As L_y continues to increase, the coupling coefficients weaken, thereby preventing the excitation of CSRRs modes by the TE_{101} or TE_{201} modes, resulting in the inability to form a four-band response. Since the CSRRs are not coupled to the TE_{102} and TE_{202} modes, the third passband is nearly unaffected by L_y. The coupling coefficient M_{ij} ($j > i$) can be calculated using Equation (7).

$$M_{ij} = \frac{f_j^2 - f_i^2}{f_j^2 + f_i^2} \tag{7}$$

where f_j and f_i ($j>i$) denote the corresponding frequencies of the proposed resonant cavity. Figure 9(b) displays the 3 dB bandwidth and resonant frequencies of the four passbands influenced by the offset L_y. With an increase in the value of L_y from 7.0 mm to 9.5 mm, the resonant frequency of the third passband remains constant. Nonetheless, the resonant frequencies of the remaining passbands are slightly disturbed. Specifically, the resonant frequency of the first and fourth passbands increases, whereas the resonant frequency of the second passband decreases. The relative bandwidths of the first three passbands undergo slight changes, while the fourth passband starts to decrease and stabilize. This theory can be applied to compensate changes in bandwidth.

4. PROCESSING AND TESTING OF CONTROLLABLE MULTIMODE FOUR-PASS BAND FILTERS

The paper proposes a four-passband filter utilizing a Rogers RT/Duroid 5880 substrate with specific parameters: a substrate thickness of 0.508 mm, a dielectric constant of 2.2, and a loss angle tangent of 0.0009. The optimized parameters, as delineated in Table 2, were derived through simulation and optimization employing the three-dimensional electromagnetic simulation software, Ansys Electronics Desktop.

The results of the actual filter, simulations, and measurements are presented in Figure 10. The vector network analyzer was employed for measurements, and the simulation results were found to be consistent with the measured results. As the filter designed in this study is a passive filter, only the S-parameters were tested, and no signal-to-noise ratio (SNR) test was required. The sources of measurement error include transmission line inaccuracies and physical joint discrepancies; however, temperature and humidity were found to have

TABLE 2. Filter size parameters.

Parameters	Value (mm)	Parameters	Value (mm)	Parameters	Value (mm)	Parameters	Value (mm)	Parameters	Value (mm)
L_1	20	W_1	34	R_1	1.1	P_1	2.5	W_g	0.4
L_s	2.3	W_s	0.8	R_2	3.8	P_2	1.0	W_c	0.6
L_y	8.1	W_d	0.4	P	1.0	d	0.6	t_i	4.0

TABLE 3. Parameter comparison between this paper and other multi-passband filters.

Ref.	Passbands	F_0 (GHz)	IL (dB)	RL (dB)	FBW (%)	TZs	Size λ_g^2
SIR microstrip line structure filter							
[1]	3	1.85/2.59/3.43	1.24/1.72/1.80	> 15	8.5/4.1/6.5	6	0.19
[4]	2	2.79/3.90	0.96/3.00	> 18	5.6/6.7	3	0.34
[6]	4	2.22/3.66/5.63/7.52	0.32/0.41/1.38/0.43	> 20	10/8/4/10	2	0.02
[7]	2	4.26/6.26	1.09/1.61	> 21	7.3/2.4	3	-
[27]	4	5.75/7.58/9.56/12.14	2.44/2.28/2.33/2.78	> 20	1.65/2.44/1.78/3.65	4	-
Double-layer substrate integrated waveguide filter							
[8]	2	9.01/11.77	1.47/1.02	> 30	10.22/8.81	2	1.21
[9]	4	11.63/12.47/13.51/14.35	0.89/1.27/1.45/1.79	> 15	1.71/1.68/1.38/1.22	6	1.56
[20]	3	11.92/13.23/14.1	1.81/2.35/1.93	> 15	2.85/1.29/1.42	6	2.72
[21]	3	1.83/2.1/2.47	2.31/2.25/3.01	> 15	3.01/2.86/2.31	6	0.05
[23]	4	7.92/8.61/10.24/11.54	2.18/2.39/1.84/1.61	> 15	1.64/1.5/2.34/1.99	6	1.06
Double-layer substrate integrated waveguide filter							
[9]	4	11.53/12.51/14.7/15.22	1.33/1.22/1.43/1.53	> 14	1.43/1.42/1.14/1	7	2.73
[10]	3	2.33/5.08/29.6	0.75/0.89/2.8	> 20	17.6/11.81/7.7	1	0.10
[14]	3	13/14/15	1.71/1.80/2.29	> 16	4.06/3.31/2.82	3	4.03
[20]	3	11.18/12.6/13.33	0.55/1.56/1.78	> 19	3.93/1.91/1.43	6	3.04
[22]	4	11.96/12.96/13.95/14.94	1.72/1.09/1.65/1.24	> 15	-	3	2.19
[23]	3	7.55/9.3/10.81	2.8/2.5/2.15	> 16	1.19/1.83/3.15	4	1.06
This	4	7.47/9.84/11.02/12.65	2.47/2.41/1.32/1.96	> 18	0.80/1.32/4.17/3.32	6	0.49

Ref.: Reference; F_0: center frequency; FBW: fractional bandwidth; TZs: Transmission zeros at lower and upper bandpass edges; λ_g: the guided wavelength at 7.47 GHz.

no significant effect [26, 27]. The simulated and measured center frequencies are 7.56/7.47, 10.02/9.84, 11.22/11.02 and 12.92/12.65 GHz, respectively, with corresponding relative bandwidths of 1.46/0.80, 1.80/1.32, 4.28/4.17, and 3.79/3.32%. Maximum in-band insertion losses are 0.92/2.47, 1.28/2.41, 0.50/1.32, and 0.63/1.96 dB, while return losses are 28.89/18.30, 21.89/27.32, 21.88/21.74, and 30.69/18.85 dB, respectively. Filter dimensions are $0.91\lambda_g \times 0.54\lambda_g$. The filter demonstrates robust out-of-band rejection, revealing six transmission zeros outside the passband, with the highest frequency point measured at -56.65 dB.

To demonstrate the advantages of the controllable four-passband filter, we compare it with the multi-passband filter as depicted in Table 3. Given the scarcity of journals and papers concerning four-passband filters, we have conducted a comparison with the multi-passband filter. The comparison of each column in Table 3 shows that the four-passband filter designed in this paper enables multi-passband transmission with a return loss greater than 18 dB and six transmission zeros. Furthermore, the filter does not require complex physical processing and has a dimensional accuracy of only one decimal place and a size of only $0.49\lambda_g^2$.

5. CONCLUSION

This paper introduces a substrate-integrated waveguide cavity perturbed by metal holes. Two complementary symmetric open resonant rings are incorporated to formulate a four-passband filter with adjustable frequency and bandwidth. The filter can selectively transmit a specific signal frequency, facilitating the extraction of the target signal from the mixed signals received in the system, thereby suppressing unwanted frequency components and mitigating the effects of interference. The four-passband filter exhibits outstanding rejection within both in-band and out-of-band frequencies, leading to heightened transmittance within a specific frequency range and an elevated blocking rate at other frequencies. This characteristic prevents interference from extraneous frequencies that may adversely impact the radar system's performance. In the receiving phase, the filter can selectively eliminate noise. The filter permits only the passage of the target signal, concurrently suppressing noise and enhancing the signal-to-noise ratio. This aspect is pivotal for precise target detection and tracking in radar and satellite communication systems. To attain the requisite high resolution for radar systems, the center frequency and bandwidth of the four-passband filter must be meticulously chosen. The narrow-band characteristics of the filter assist in precisely discriminating between distinct targets and enhancing the radar system's target resolution.

ACKNOWLEDGEMENT

This work was supported by 2023 Liaoning Provincial Department of Education Basic Research Project (JYTMS20230818): Research on Multi-band Millimeter-wave Filter for 5G Wireless Communication; Liaoning Provincial Applied Basic Research Program Project (2022JH2/101300275): Design and Research on 5G Millimeter-wave Array Antennas, and National Natural Science Foundation of China Upper-level Project (61971210): Support for Future-oriented Wireless Reconfigurable Intelligent RF Module and Neural Network Modeling Research.

REFERENCES

[1] Wang, M., "Research and design of multi-band microstrip filters," Ph.D. dissertation, Ph.D. dissertation, Xi'an Technological University, Xi'an, Shaanxi, China, 2023.

[2] Alvi, T. S., M. H. Ahsan, M. Ali, F. Ramzan, K. A. Aljaloud, A. H. Alqahtani, R. Hussain, A. Alomainy, and M. Q. Mehmood, "A high-performance, low-cost, and integrated hairpin topology RF switched filter bank for radar applications," *Sensors*, Vol. 24, No. 2, 434, 2024.

[3] Yang, Q., X. Zuo, S. Guo, and Y. Zhao, "Evaluation of InSAR tropospheric delay correction methods in the plateau monsoon climate region considering spatial-temporal variability," *Sensors*, Vol. 23, No. 23, 9574, 2023.

[4] Wu, Y. and X. Wang, "E-type tunable multi-branch SIR dual-band filter," *Journal of Microwaves*, Vol. 32, No. S1, 230–233, 2016.

[5] Kim, B. S., J. W. Lee, and M. S. Song, "An implementation of harmonic-suppression microstrip filters with periodic grooves," *IEEE Microwave and Wireless Components Letters*, Vol. 14, No. 9, 413–415, 2004.

[6] Zhang, Y., Y. Fang, and G. Wu, "Design of a novel quad-band filter based on multi-sirs," *Progress in Solid State Electronics*, Vol. 41, No. 01, 29–34, 2021.

[7] Fan, J., S. Qiao, L. Zhang, and e. al., "Design of dual-band filter based on folded SIR resonator," *Journal of Microwaves*, Vol. 39, No. 04, 50–53, 2023.

[8] Zheng, Y. and Y. Dong, "Dual-band, dual-mode, microstrip resonator loaded, compact hybrid SIW bandpass filter," in *2021 IEEE MTT-S International Microwave Symposium (IMS)*, 50–53, Atlanta, GA, USA, 2021.

[9] Zhou, K., C.-X. Zhou, H.-W. Xie, and W. Wu, "Synthesis design of SIW multiband bandpass filters based on dual-mode resonances and split-type dual-and triple-band responses," *IEEE Transactions on Microwave Theory and Techniques*, Vol. 67, No. 1, 151–161, Jan. 2019.

[10] Zheng, S. Y., Z. L. Su, Y. M. Pan, Z. Qamar, and D. Ho, "New dual-/tri-band bandpass filters and diplexer with large frequency ratio," *IEEE Transactions on Microwave Theory and Techniques*, Vol. 66, No. 6, 2978–2992, Jun. 2018.

[11] Zhu, Y. and Y. Dong, "A compact dual-band quasi-elliptic filter based on hybrid SIW and microstrip technologies," *IEEE Transactions on Circuits and Systems II: Express Briefs*, Vol. 69, No. 3, 719–723, Mar. 2022.

[12] Chen, X.-P., K. Wu, and Z.-L. Li, "Dual-band and triple-band substrate integrated waveguide filters with Chebyshev and quasi-elliptic responses," *IEEE Transactions on Microwave Theory and Techniques*, Vol. 55, No. 12, 2569–2578, Dec. 2007.

[13] Li, P., H. Chu, and R.-S. Chen, "Design of compact bandpass filters using quarter-mode and eighth-mode SIW cavities," *IEEE Transactions on Components, Packaging and Manufacturing Technology*, Vol. 7, No. 6, 956–963, Jun. 2017.

[14] Xie, H.-W., K. Zhou, C.-X. Zhou, and W. Wu, "Substrate-integrated waveguide triple-band bandpass filters using triple-mode cavities," *IEEE Transactions on Microwave Theory and Techniques*, Vol. 66, No. 6, 2967–2977, Jun. 2018.

[15] Zhu, X.-C., W. Hong, K. Wu, H.-J. Tang, Z.-C. Hao, J.-X. Chen, and P. Chu, "Design and implementation of a triple-mode planar filter," *IEEE Microwave and Wireless Components Letters*, Vol. 23, No. 5, 243–245, May 2013.

[16] Zhang, D.-D., L. Zhou, L.-S. Wu, L.-F. Qiu, W.-Y. Yin, and J.-F. Mao, "Novel bandpass filters by using cavity-loaded dielectric resonators in a substrate integrated waveguide," *IEEE Transactions on Microwave Theory and Techniques*, Vol. 62, No. 5, 1173–1182, May 2014.

[17] Liu, Z., G. Xiao, and L. Zhu, "Triple-mode bandpass filters on CSRR-loaded substrate integrated waveguide cavities," *IEEE Transactions on Components, Packaging and Manufacturing Technology*, Vol. 6, No. 7, 1099–1105, Jul. 2016.

[18] Zhao, Y., C. Zhou, and e. al., "Design of quadruple-band filter based on substrate-integrated waveguide," *Journal of Microwaves*, Vol. 33, No. S1, 152–156, 2017.

[19] Lee, B., G. Lee, and J. Lee, "Two-layered cross-coupled post-loaded SIW filter with microstrip ports," *IEEE Transactions on Circuits and Systems II: Express Briefs*, Vol. 70, No. 4, 1346–1350, Apr. 2023.

[20] Li, D., X. Chen, W. Luo, Z. Zheng, and Q. Chen, "Compact tri-band SIW bandpass filters with high selectivity and controllable center frequencies using perturbation structure," *IEEE Transactions on Circuits and Systems II: Express Briefs*, Vol. 70, No. 11, 4043–4047, Nov. 2023.

[21] Ho, M.-H. and K.-H. Tang, "Miniaturized SIW cavity tri-band filter design," *IEEE Microwave and Wireless Components Letters*, Vol. 30, No. 6, 589–592, Jun. 2020.

[22] Guo, X., L. Zhu, and W. Wu, "Design method for multiband filters with compact configuration in substrate integrated waveguide," *IEEE Transactions on Microwave Theory and Techniques*, Vol. 66, No. 6, 3011–3018, Jun. 2018.

[23] Li, D., W. Luo, X. Chen, Y. Liu, K.-D. Xu, and Q. Chen, "Miniaturized dual-/tri-/quad-band bandpass filters using perturbed multi-mode SIW cavity," *IEEE Transactions on Components, Packaging and Manufacturing Technology*, Vol. 13, No. 10, 1685–1693, Oct. 2023.

[24] Zhou, C., H. Dong, J. Wang, and e. al., "Development of high-performance millimeter-wave CSRR-SIW bandpass filter," *Journal of Hangzhou Dianzi University (Natural Science Edition)*, Vol. 42, No. 02, 8–13, 2022.

[25] Gan, H., "Design of high-performance and miniaturized planar microwave sensor based on complementary split ring res-

onator (CSRR)," Ph.D. dissertation, Hangzhou Dianzi University, Hangzhou, Zhejiang, China, 2022.

[26] Gao, M., X. Zhang, X. Chen, and J. Nan, "Design of double-notch UWB filter with upper stopband characteristics based on ACPW-DGS," *PLoS ONE*, Vol. 18, No. 2, e0282060, 2023.

[27] Wurihan, "Research and implementation of multi-bandpass filters," Master dissertation, University of Electronic Science and Technology of China, Chengdu, Sichuan, China, 2023.